Experimental study of nanofiber production through forcespinning

Simon Padron, Arturo Fuentes, Dumitru Caruntu, and Karen Lozano[a)]
Department of Mechanical Engineering, The University of Texas Pan American, Edinburg, Texas 78539, USA

(Received 21 June 2012; accepted 19 November 2012; published online 11 January 2013)

A newly developed method of producing nanofibers, called forcespinning, has proven to be a viable alternative to mass produce nanofibers. Unlike electrospinning, the most common method currently being employed (which draws fibers through the use of electrostatic force), forcespinning utilizes centrifugal forces which allow for a host of new materials to be processed into nanofibers (given that electric fields are not required) while also providing a significant increase in yield and ease of production. This work presents a detailed explanation of the fiber formation process. The study is conducted using high speed photography to capture the jet initiation process at the orifice and to track the trajectories of the resulting jets. The effects that influential controllable parameters have on the fiber trajectories and final fiber diameters are presented. The forcespinning controllable parameters include the spinneret angular velocity and aspect ratio, orifice radius and orientation, fluid viscoelasticity and surface tension, fluid fill level, solvent evaporation rate, temperature, and distance of spinneret orifice to collector. © *2013 American Institute of Physics*. [http://dx.doi.org/10.1063/1.4769886]

I. INTRODUCTION

Forcespinning (FS) has proven successful as a viable method to mass produce polymeric nanofibers. Unlike electrospinning, which draws fibers through the use of electrostatic forces, FS utilizes centrifugal forces which allow for a significant increase in yield and ease of production. The fiber production rate has been shown to be over 1 g/min per nozzle in the lab scale units; this yield is significantly higher than any lab scale electrospinning apparatus where typical systems operate at about 0.1 g/h (considering typical feeding rates of hundreds of microliters/minute). No electric fields are needed; therefore, restrictions[1] imposed on materials with low dielectric constants are eliminated (e.g., fluoropolymers). Also, FS has the distinct advantage of being able to produce nanofibers of both polymeric solutions and melts. The FS process begins by first loading the solution/melt into a spinneret, specially designed for this process. During the nanofiber production, the polymer solution is drawn from the orifice by rotating forces.[2] As the polymer is drawn, the important parameters that need to be considered include: spinneret angular velocity and orifice radius, polymer viscoelasticity (which includes viscosity and relaxation time of the material), surface tension, evaporation rate (for solvent in solution) and temperature (melting and solidification), and distance of spinneret orifice to collector. The rate of solvent evaporation has an effect on polymer viscosity and elasticity.[3] In the case of polymer solutions, it is important to determine the polymer-solvent compatibility in order to determine optimum concentrations that will allow the production of nanofibers with the desired size and morphology. In the case of forcespinning of melts, it is important to determine the optimum temperature that will provide a viscosity that will allow the melt to flow and produce nanofibers.

In order to produce a polymer jet, the rotating forces must be high enough to overcome the surface tension of the solution or melt. If the forces exerted on the jet are too high, the surface tension of the polymer solution is capable of causing the jet to break up and produce beads. This may occur in certain conditions where the angular velocity of the spinneret is low (low centrifugal forces) and/or the viscosities are not too high.

Another property that must be controlled for successful fiber formation is the viscosity of the polymer melt or solution. If the viscosity is high the forces being used to draw the fiber may not be strong enough to create a jet. On the other hand, if the viscosity is low, the jet may break up and produce beads instead of fibers. Given the low chain entanglement associated with low viscosities (high melt flow index) the possibility also exists for the production of beaded nanofibers. The viscoelasticity of the polymer gives rise to phenomena such as extrudate swelling, which increases the diameter of the jet as it is pulled through the orifice. This phenomenon is explained by stress relaxation due to the elastic component of the polymer.[3] The viscoelastic properties also give rise to instabilities as the fiber is reduced in size and the solvent begins to evaporate.

The evaporation rate of the polymer solution jet is also an important parameter. As the jet is expelled from the orifice and accelerated toward the collector, the fiber experiences rapid evaporation which also reduces the diameter of the fiber. If the evaporation rate of the solvent is too low, then the fibers may be converted into a thin film as the layers build up on the collector and the still wet fibers merge. If the evaporation rate is relatively high, then the elongation process of the polymer jet is disturbed and fibers with large diameters are produced. This is dependent of various factors such as the vapor pressure, boiling point, specific heat, enthalpy, rate of heat supply, interaction between solvent and solute molecules, surface tension of liquid, and air movement on the liquid surface.[3]

The diameter of the orifice from which the polymer solution is drawn has an effect on nanofiber production processes. For example, in Mo *et al.*,[4] a smaller diameter was found to

[a)]Electronic mail: lozanok@utpa.edu.

reduce clogging and the amount of beads on fibers using the electrospinning method. The decrease in orifice diameter also reduced the overall diameter of the fibers. The orientation and geometry of the orifice also has an effect on the fiber formation and is studied in detail in the following sections.

In electrospinning, the distance to the collector plays a crucial role, since increasing or decreasing the distance between the needle and collector also increases or decreases the forces drawing the fiber from the needle, respectively. In FS, choosing the distance of the collector does not affect the body forces on the fiber as it travels; therefore, choosing the optimum distance is based solely on how long it take for the solvent to evaporate, the distance required to allow the fiber to begin to spiral outwards, and the type of collection method used. If the distance of the collector is relatively short, the fiber will not be allowed to stretch and a larger diameter will be obtained; once this critical distance is surpassed the collector distance becomes a less crucial component and the reduction in fiber diameter with increasing distance becomes minimal.

The modeling of the fiber formation is therefore based on the angular velocity of the spinneret, viscoelastic properties of the polymer, collector diameter, radius of the orifice, and solvent evaporation rate. In certain methods of fiber deposition, the effects of gravity may also have an effect on the formation of the fibers. Using a rotating reference for the coordinate system, the governing equations of the system may be described by the continuity equation:

$$\nabla \bullet u = 0, \tag{1}$$

where $\boldsymbol{u}$ is the relative velocity of the fiber jet, and the Cauchy momentum equations

$$\frac{\partial \boldsymbol{u}}{\partial t} + (\boldsymbol{u}\bullet\nabla)\boldsymbol{u} = -\frac{\nabla P}{\rho} + \boldsymbol{g} + \frac{\nabla \boldsymbol{T}}{\rho} - \boldsymbol{\omega} \times (\boldsymbol{\omega} \times \mathbf{r}) - 2\boldsymbol{\omega} \times \boldsymbol{u}, \tag{2}$$

where P is the pressure, $\boldsymbol{g}$ is the gravity vector, $\boldsymbol{T}$ is the stress tensor, $\boldsymbol{\omega}$ is the angular velocity of the spinneret, and $\mathbf{r}$ is a position vector describing a point along the fiber. In this case, the effects due to aerodynamic forces on the fiber are exempted. The viscoelastic component depends on the polymer properties and is most basically described by the stress tensor, strain-rate tensor, polymer viscosity, and polymer relaxation time. The nondimensional form of the equations provides some important dimensionless numbers that give the ratios between the various forces in the system. Some of these include the Reynolds number (ratio of inertial to viscous forces), Froude number (ratio of inertial to gravitational force[5]), Weber number (inertial force to surface tension[5]), Rossby number (ratio of inertial to Coriolis force[6]), and Deborah number (polymer relaxation to flow time[5]). The Deborah number can be used to select appropriate viscoelastic models. The Pipkin diagram[7] provides a method for determining which mathematical model would be appropriate for the representation of a polymer being stretched at high rates. For the FS method, large deformations are experienced in a short period of time, in which case non-linear viscoelastic models such as the upper-convected Maxwell, Phan-Thien Tanner, and Geisiekus models must be used to approximate the solution or melt material properties. An inviscid two dimensional model of fluid dynamics of force-spinning is reported in the literature.[10]

This work makes use of high speed photography to provide an insight into what occurs during the initial stages of fiber formation and to provide detailed information on the propagation of the produced fibers as they approach the collector. The trajectories of the resulting fibers are plotted and compared as various parameters are varied. These results are then compared to the resulting fiber diameters. Understanding the mechanisms of nanofiber formation by the FS method will support the optimal selection of material properties (viscosity, surface tension, etc.), operating parameters (e.g., angular velocity, temperature, etc.), and machine components/devices (e.g., spinnerets, collectors, etc.).

II. EXPERIMENTAL SETUP

A Phantom Vision v12.1 high speed camera, with three NorthStar high intensity 120 W lamps, was used. Various angles and magnifications were used to obtain the desired images which included top, angle, side, and tip close-up views of the system. The capture rates ranged from 1500 to 11 000 frames/s, depending on the operating angular velocity of the system, with frame rates set for image capture at every 5° of spinneret rotation. This work evaluated the jet initiation and fiber trajectories for solution based polymeric systems. Polyethylene oxide (PEO) dissolved in deionized water was used. The polymer concentration in the solution varied from 6 to 10 wt. %. First, the initiation of the solution jet was studied by capturing close-up views of the orifices. The magnification used was 20×, using a 10× magnification lens with extension tubes. For the capture of fiber trajectories, angled and top view setups were used. The top view setup is shown in Figure 1. The effects of changing parameters, such as angular velocity, orifice geometry, aspect ratio of the orifice, polymer concentration, and fluid fill level, on the trajectories and final fiber diameters were examined. Needles were used in order to easily customize the nozzle geometry and orientation. The resulting fibers were imaged using a Zeiss Sigma VP scanning electron microscope (SEM).

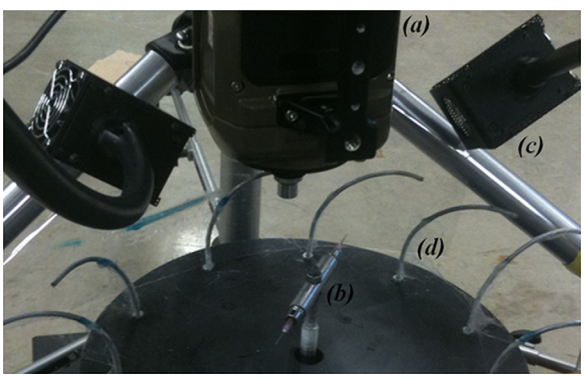

FIG. 1. High speed photography setup: (a) high speed camera, (b) spinneret, (c) lamp, (d) collector.

III. RESULTS AND DISCUSSION

A. Jet initiation

The formation of the jet by the FS process from 0 to 4500 rpm is shown in Figure 2(a) (clockwise direction of rotation). The orifice diameter used to image the jet shape at exit is 838 μm. As the spinneret accelerates, a pendant drop is seen to originate from the orifice due to the centrifugal forces experienced on the fluid within the spinneret, shown in Figure 3(a), with O being the center of rotation, d the distance of the center of mass, CM_1, to the center of rotation (O), CM_2, being the center of mass of the volume within the reduced diameter section, and ℓ the fluid level up to the orifice. Setting the forces in equilibrium and using the Darcy-Weisbach equation provides the exit velocity (U)

$$U = \Omega \sqrt{\frac{2k\left(D - \frac{k}{2}\right) + 2L\left(C - \frac{L}{2}\right)}{1 + f\frac{L}{2r}}}, \tag{3}$$

where Ω is the angular velocity of the spinneret, L is the reduced diameter length, C is the radius of the spinneret, D is the distance of the reservoir wall from the center of rotation, k is the fluid level up to the reservoir wall, r is the radius of the orifice, and f is the friction factor due to the head losses experienced along the reduced diameter path. For systems in which the Reynolds number (Re) is small, the friction factor can be derived from the Hagen-Poisseuille equation, $f = 64/\mathrm{Re}$. If the container is considered to have continuous feed, then the equation is reduced to

$$U = \Omega \sqrt{\frac{D^2 + 2L\left(C - \frac{L}{2}\right)}{1 + \frac{32L}{\mathrm{Re}\, r}}}. \tag{4}$$

The equation for continuous feed (Eq. (4)) can then be solved for using the quadratic equation with Reynolds number defined as $\mathrm{Re} = 2\rho U r/\mu$, where μ is the viscosity of the material. Thus

$$U = -\frac{8L\mu}{\rho r^2} + \frac{1}{2}\sqrt{256\left(\frac{L\mu}{\rho r^2}\right)^2 + 4\Omega^2\left[D^2 + 2L\left(C - \frac{L}{2}\right)\right]}. \tag{5}$$

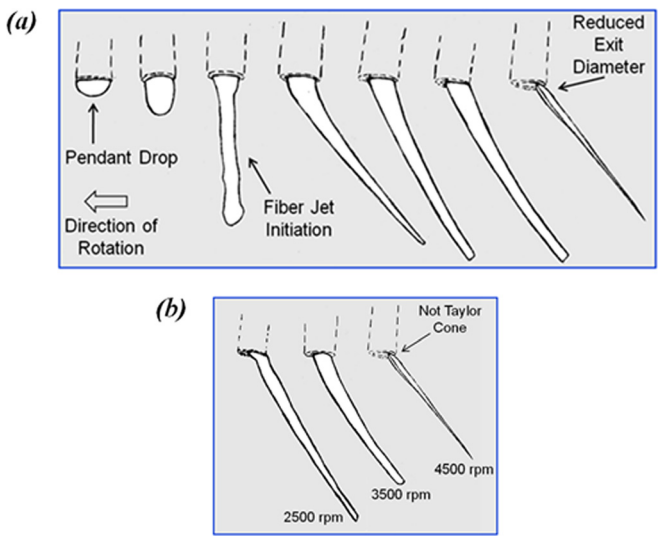

FIG. 2. (a) Evolution of jet at orifice for fiber production through forcespinning as it accelerates to 4500 rpm, (b) jet shape at different angular velocities.

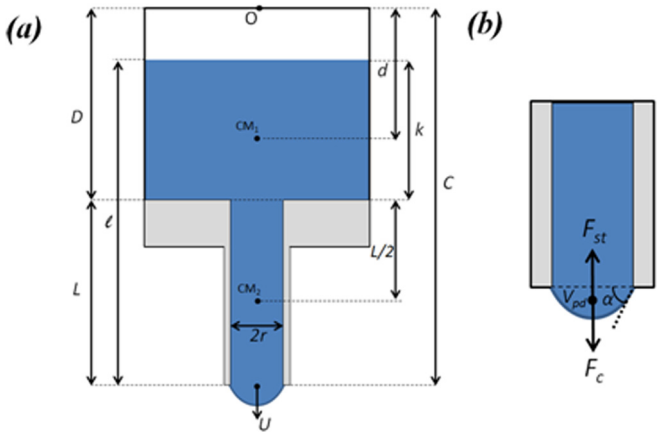

FIG. 3. Initial forces on material: (a) forces within spinneret, (b) forces on the pendant drop.

At the orifice, the pendant drop does not travel outward at low angular velocities due to the equilibrium between the surface tension of the solution, F_{st}, and the centrifugal force, F_c, shown in Figure 3(b). After a critical angular velocity is reached, the formed jet begins to travel outward on a curved trajectory. Setting the forces on the pendant drop in equilibrium and solving for the critical angular velocity gives

$$\Omega_c = \sqrt{\frac{2\pi r\sigma \sin\alpha}{\rho V_{pd} C}}, \tag{6}$$

where $2\pi r$ is the perimeter of the orifice, σ is the surface tension, α is the contact angle of the drop right before jet initiation occurs, ρ is the density of the solution, V_{pd} is the volume of the pendant drop, and C is the radius of the spinneret. This in turn provides the critical exit velocity, U_{cr}, by substituting the angular velocity in Eq. (5) with Eq. (6)

$$U_{cr} = -\frac{8L\mu}{\rho r^2} + \frac{1}{2}\sqrt{256\left(\frac{L\mu}{\rho r^2}\right)^2 + \frac{8\pi r\sigma \sin\alpha}{\rho V_{pd} C}\left[D^2 + 2L\left(C - \frac{L}{2}\right)\right]}. \tag{7}$$

Once a jet is initiated and the angular velocity continues to increase, the diameter of the jet at the orifice begins to decrease, due to the extensional forces, until it reaches a diameter considerably smaller than the orifice diameter, as seen in the last sketch of Figure 2(a).

The FS jet initiation process when compared to electrospinning has the distinct differences of having an initially curved jet, and instead of a Taylor cone being produced, the jet at exit is reduced considerably in size and is expelled on

the trailing end of the orifice, making the initial jet diameter dependent on the curvature of the orifice on which the exiting jet makes contact. Therefore, small variations in orifice diameter do not play a significant role in the initial jet diameter. From experimental data and SEM imaging it has been established that there exist certain angular velocities that produce nanofibers depending on the material properties and system setup.[8] To determine the effect that the reduction in exit diameter of the jet has on the resulting fiber diameter, the initial jet shape at the orifice after reaching constant speed was obtained at three different angular velocities, shown in Figure 2(b). For the solution used, 10 wt. % PEO in H_2O, it is known that nanofibers are produced at angular velocities higher than 4000 rpm. By examining the shape of the jet at the orifice above 4000 rpm, it is determined that nanofiber production using the FS method is aided by the fact that the diameter of the jet at exit is reduced well below the diameter of the orifice. The reason for the reduction of the initial diameter of the jet to well below the orifice radius can be attributed to the extensional forces experienced by the jet as it is expelled outward on a curved path and the amount of fiber being pulled along as the spinneret rotates. These extensional forces affect the jet at exit by reducing its initial diameter and increase the initial exit velocity of the jet. Once steady state is reached, the exit velocity of the jet may be described by introducing the velocity increase from the extensional forces to Eq. (5) to give

$$U = U_f - \frac{8L\mu}{\rho r^2} + \frac{1}{2}\sqrt{256\left(\frac{L\mu}{\rho r^2}\right)^2 + 4\Omega^2\left[D^2 + 2L\left(C - \frac{L}{2}\right)\right]}, \tag{8}$$

where U_f is the velocity increase associated with the fiber pulling force.

These results show that two critical angular velocities exist; the first is the critical velocity that produces a jet and the second is the critical velocity that reduces the solution below the orifice diameter and exits along the backside of the orifice wall. The insight obtained into the initial solution diameter must be used when considering the modeling of the system. Mellado *et al.*[9] in their calculations for their similar rotary-jet spinning method assume that the original jet radius is that of the orifice. Although this may be true for solutions at low angular velocities and/or low viscosities, it is not valid when dealing with nanofiber formation for which higher viscosities and angular velocities are required. Instead, the jet radius at the orifice must be made dependent on the parameters involved in FS such as the angular velocities, spinneret geometry, and material properties.

B. Extension process

For fiber size optimization, collection purposes, and computer models, it is of interest to know in detail how the fiber extension process occurs during forcespinning. Currently, the FS collection methods include a radial collection method (using vertical prongs), a substrate deposition method, and a spooling collection method that aligns the nanofibers together into yarns. The setups used for this study included the radial collection method. An example of the FS process is shown at an angle in Figure 4(a) and a time-lapse top view is shown in Figure 4, showing multiple superimposed images of a single needle as it rotates and expels the solution.

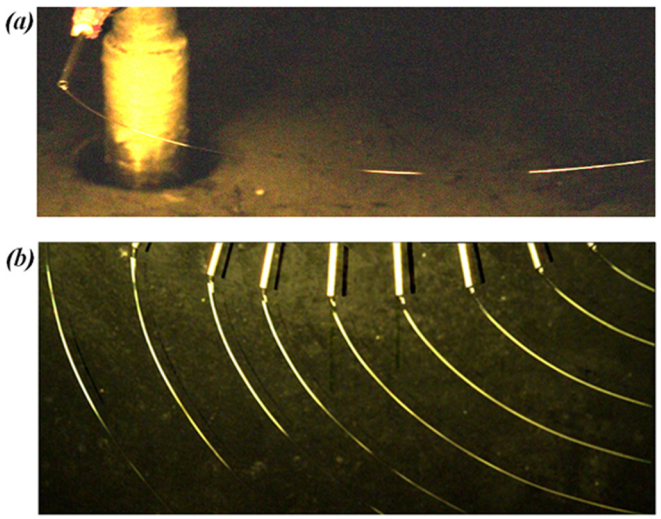

FIG. 4. Fiber produced through forcespinning: (a) angled view (b) time-lapse top view.

A general trajectory of a forcespun fiber is shown in Figure 5. The solution used was 8 wt. % PEO in H_2O, with a 260 micron inner diameter needle, forcespun at 4000 rpm. The general trajectory of the fibers as they are being produced starts with the jet being expelled outwards, then almost immediately it is pulled inwards until it reaches a stationary radial distance from the center of rotation for a few spinneret rotations, during which the fiber continues to be stretched. Depending on the material and angular velocity of the spinneret, stationary stretching was observed to last between 2 and 5 spinneret rotations. Once the fiber is reduced to a certain critical diameter, the fiber again begins to expand radially outwards, due mainly to the aerodynamic forces that are produced by the spinneret, and to collect on the collector. From these observations it is deduced that for nanofiber production it is desirable for the

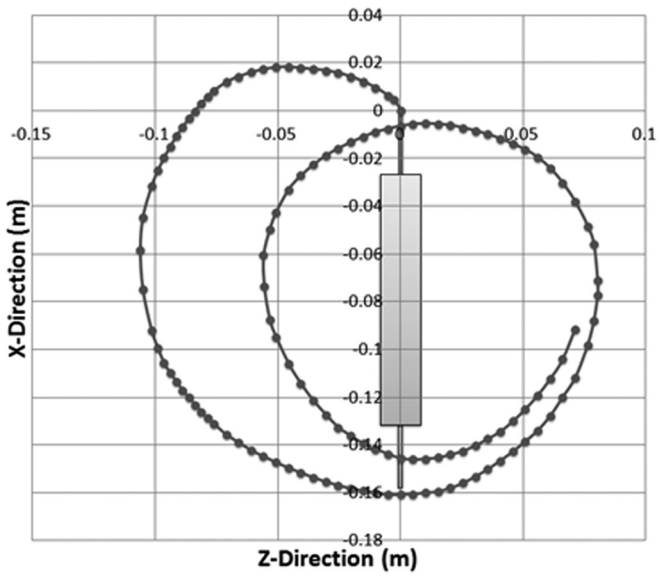

FIG. 5. Fiber trajectory of 8 wt. % PEO solution spun at 4000 rpm.

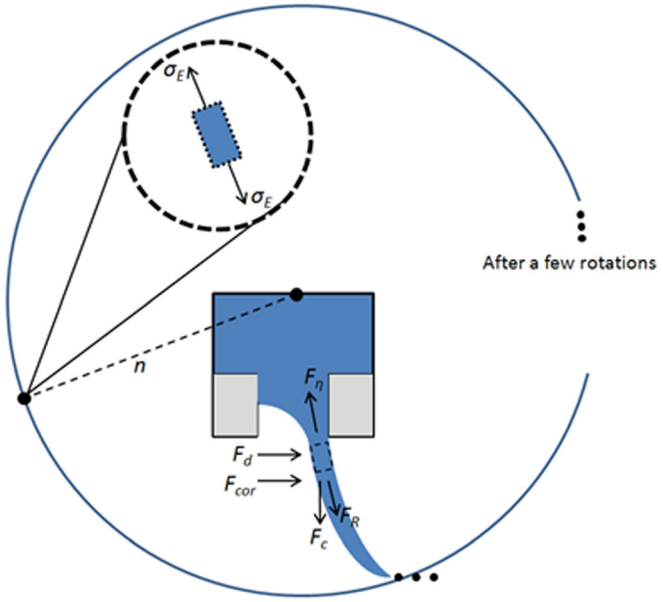

FIG. 6. Forces experienced by the fiber during travel.

fiber to orbit, so that the elongation process can occur for a longer period of time before the collector is reached. By calculating the arc length of the fiber after a few rotations as it remains at a stationary radius from the center, it is found that the length of the produced fiber is approximately 5 m long after only 4 rotations using normal operational speeds of 5000 rpm, providing an estimated production rate of 100 m/s. Since the fiber continues to stretch as it expands outwards unto the collector, it is seen that the fiber length, s, is much larger than the collector distance, D_c ($s \gg D_c$). In Mellado *et al.*[9] it is assumed that the solution experiences an elongational flow along a fixed x-direction, where the x-direction denotes the distance between the orifice and the collector. Their results may be valid for certain cases where the fiber length may be comparable to the collector distance (low viscosities, low angular velocities). In FS, it is established that at low viscosities the fiber trajectories follow a curved path outward directly onto the collector. However, as the angular velocity of the spinneret and the viscosity of the fibers are increased, the trajectory changes, producing spiral trajectories that allow the fiber to increase dramatically in length, reaching lengths much larger than their distance from the orifice to the collector.

The forces experienced by the jet as it is stretched, assuming a reference frame fixed on the rotating spinneret is shown in Figure 6, where F_d is the drag force, F_{cor} the Coriolis force, F_c the centrifugal force, F_η the viscous force, and F_R the resulting force from the Coriolis, centrifugal, and drag forces experienced by the jet. As the jet exits the orifice, the elongational forces reduce the diameter of the jet below the orifice diameter. As the jet travels outward it is pulled inwards until it reaches a distance, n, from the center of rotation. At this point, forces reach a balance where only extensional stresses, σ_E, along the arc-length of the fiber are experienced. It is assumed that initially the jet can be described as a viscous fluid, with a viscous force, F_η, described by

$$F_\eta = \frac{\eta_E A \dot{\varepsilon}}{s}, \tag{9}$$

where η_E is the elongational viscosity of the jet, A the cross-sectional area, and s the length of the jet. At large fiber lengths, once the stable position is reached the fiber is considered solid enough, due to evaporation effects, to be described by a nonlinear viscoelastic model such as the upper-convected Maxwell model. The stresses at this point may be approximated by uniaxial extensional stress

$$\sigma_E = \frac{2\eta_s \dot{\varepsilon}}{1 - 2\lambda\dot{\varepsilon}} + \frac{\eta_s \dot{\varepsilon}}{1 + \lambda\dot{\varepsilon}}, \tag{10}$$

where η_E is the shear viscosity of the material and λ is the relaxation rate. Eventually, the fiber is elongated to a point where the pulling forces become weak and the radius reduced significantly that the aerodynamic forces caused by the spinneret begin to push the fiber outwards once again, allowing it to be collected.

Another phenomenon experienced by the fiber during FS is a traveling wave disturbance caused by the aerodynamics of the spinneret. To depict the aerodynamic disturbance experienced by the fiber, a section of the fiber expelled during a previous rotation of the spinneret was chosen, and its shape was taken at 6 different moments in time as the spinneret approached it at intervals of 928 μs, shown in Figure 7.

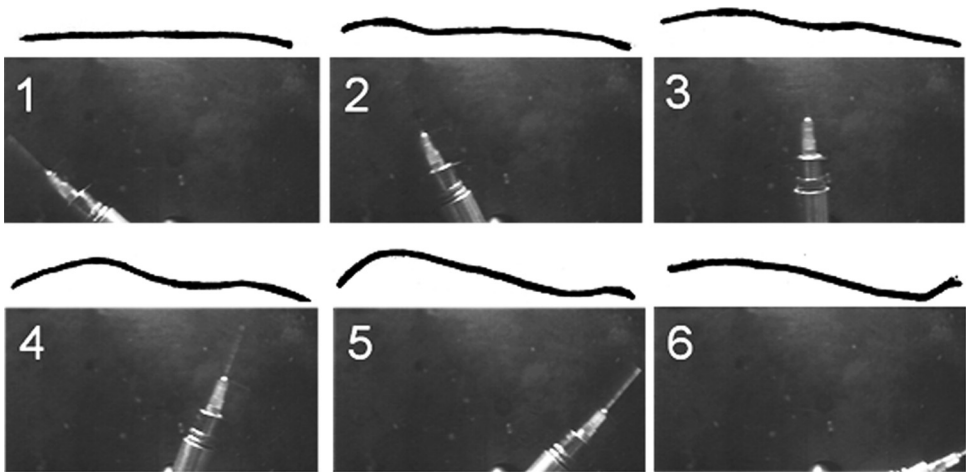

FIG. 7. Aerodynamic disturbance experienced by the fiber in successive 928 μs intervals.

As the spinneret passes by the fiber, which is approximately half an inch away from the needle, it begins to vibrate as the air being disturbed by the spinneret pushes against it, creating a traveling wave on the fiber that follows the spinneret. The produced fiber vibrations aid in the reduction of the fiber diameter as it is being stretched. However, the magnitude of the effects is still being studied.

Summarizing, *nanofiber* development can be classified into 5 processes, shown in Figure 8. Fiber formation (1) requires that a critical angular velocity, Ω_1, be reached so that a jet is produced. Once a jet is produced, it is required that a second critical angular velocity, Ω_2, be reached during which the jet diameter at exit is reduced well below the orifice diameter. These conditions have been established in the fiber formation part of this work. Afterwards, an angular velocity must be established at which the fiber reaches what will from now on be described as orbital trajectory (2). During orbital trajectory, the fiber reaches a stable position during which the fiber continues to be elongated without a significant change in its distance to the collector. It is during this period that the fiber diameter experiences the most reduction. It is also during this time that the fiber experiences vibration in the form of a traveling wave created by the aerodynamic forces from the spinneret (3). After a certain amount of spinneret rotations, the fiber diameter is reduced considerably and begins to once again expand outwards to eventually reach the collector (4). Finally, a collection method (5) is used to gather the produced fibers. Depending on whether the fibers are being collected radially, on a substrate, or through the spooling method, the fiber extension process may be affected. Having the collector too close to the spinneret will interfere with fiber formation by not allowing full extension of the fiber. However, once the distance of the collector is beyond that needed for the fiber to be expelled and pull inwards into orbit, the effects that distance of the collector has on final diameter size is minimized since most diameter reduction occurs within this region.

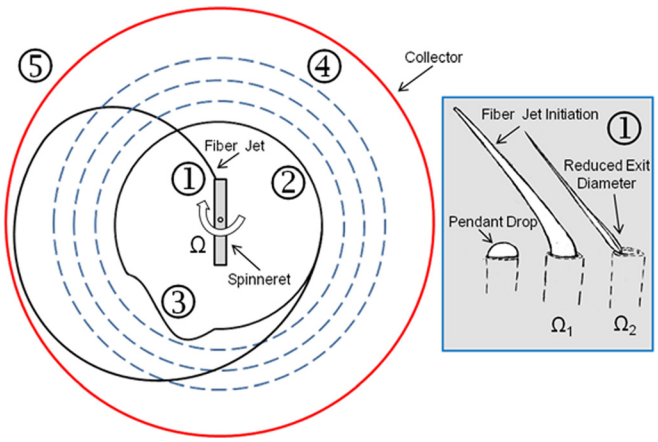

FIG. 8. Forcespinning fiber extension process: ① jet exit, ② orbital trajectory, ③ fiber vibration from aerodynamic disturbance, ④ orbital expansion, ⑤ fiber collection method.

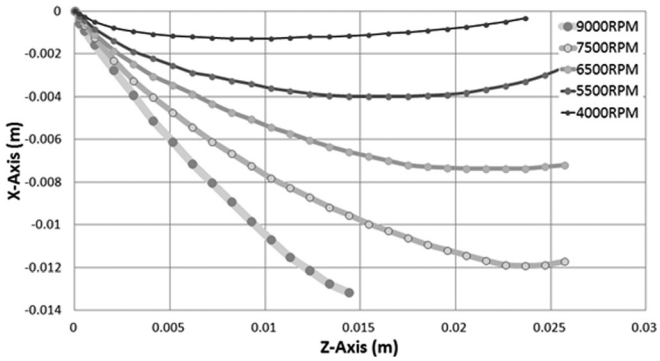

FIG. 9. Fiber trajectories with varying angular velocities.

C. Effects of changing parameters on fiber initiation and trajectories

The effects of the controllable parameters on fiber trajectory and final fiber diameter in FS are now studied. All of the following recorded trajectories and fiber diameters were obtained using an orifice diameter of 159 μm. The results from varying the spinneret angular velocity between 4000 rpm and 9000 rpm (Figure 9) show that as the angular velocity is increased, the fiber trajectory expands further outward. It is also determined that a critical angular velocity must be reached so that the fibers can be collected and not be pulled back onto the rotating shaft. For example, for the 6 wt. % PEO solution used in Figure 9, fiber collection occurred at and above 2500 rpm; below that, the fibers were pulled in and collected on the rotating shaft. Comparing the trajectory results to the fiber diameters produced, shown in Table I, it is seen that as the angular velocity is increased and the trajectory is expanded, the fiber diameters are reduced, and the fibers produced become more uniform in size, with a sample standard deviation of 30 nm at 6000 rpm. There is also an upper threshold, at which the angular velocity becomes relatively large and jet break-up occurs.

The next parameter that was varied was the viscosity of the solution. Three different PEO concentrations were used: 6 wt. %, 8 wt. %, and 10 wt. %, all dissolved in water; these solutions were forcespun at an angular velocity of 6000 rpm. Results show that as the viscosity is increased, by increasing the PEO concentration, the trajectory of the fiber contracts and comes closer to the center, as seen in Figure 10. As the viscosity of the material was increased, the angular velocity required to collect the fibers also increased. For example, for the10 wt. % PEO solution, most of the fibers were pulled in below 4500 rpm, while for the 6 wt. % solution fiber collection began at 2500 rpm. Table II shows the resulting

TABLE I. Fiber diameters at varying angular velocities using 6 wt. % PEO.

Angular velocity (rpm)	Average fiber diameters (nm)	Sample standard deviation (nm)
2500	**315**	**115**
3500	**280**	**110**
4500	**260**	**100**
6000	**130**	**30**

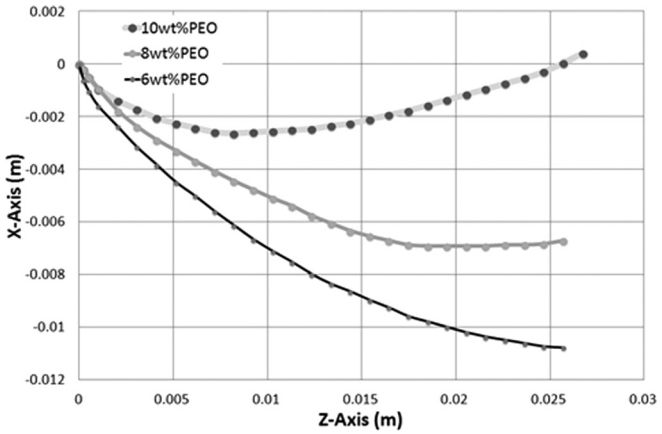

FIG. 10. Fiber trajectories with varying viscosities.

nanofibers at the different solution concentrations. Increasing the concentrations while maintaining the angular velocity constant at 6000 rpm increased the final diameter of the fibers produced.

The effects that changing the orifice orientation has on the jet exit shape and fiber trajectory were analyzed next. The focus was to determine whether there exists an optimal jet exit angle at which the final fiber diameter can be minimized. To do this, needles with varying exit angles were custom made to represent orifices at selected orientations. Four different angles were studied, with the fifth angle being a straight needle. The resulting jet shapes (using 838 μm orifice diameters) are shown in Figure 11. Figure 11(a) has an angle of 89° with respect to the straight needle and is curved in the direction opposite of rotation. From the jet images it can be seen that as the angles get closer to the straight needle the initial jet diameters increase. There also seems to be an angle at which the jet exits perpendicularly to the orifice. This angle depends on the solution properties and angular velocity. For the solution used, at 2500 rpm, the angle seems to be close to 30°, shown in Figure 11(b). This angle may prove important in applications such as coaxial fiber formation, in which it is required that dual material concentric fibers are produced. Bending the needle in the direction or rotation makes the jet increase its curvature at exit. At the largest angle of 89° (Figure 11(d)) in the direction of rotation there is a considerable reduction in the exit diameter of the jet. Comparing the initial trajectories of the different needle angles shows that as the angle increases in the direction of rotation, the trajectory of the jet expands outward, with the needle curvature of 89° in the direction of rotation having

TABLE II. Fiber diameters at varying material concentrations forcespun at 6000 rpm.

Material concentration (wt. % PEO)	Average fiber diameters (nm)	Sample standard deviation (nm)
6	**130**	**30**
8	**360**	**90**
10	**400**	**90**

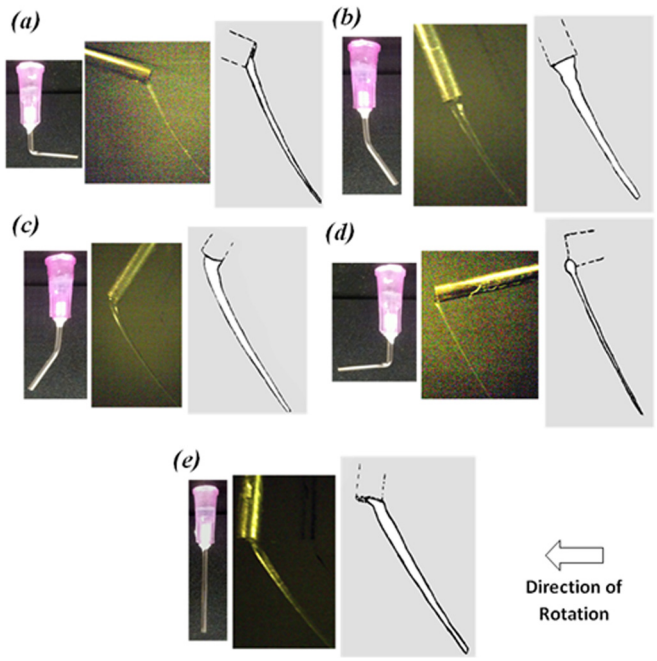

FIG. 11. Formation of various orifice exit angles (a) curved opposite of rotation 89°, (b) curved opposite of rotation 30°, (c) curved direction of rotation 30°, (d) curved direction of rotation 89°, (e) straight needle.

the most outward trajectory and the needle curvature of 89° opposite of rotation having the most contracted initial path, shown in Figure 12.

The resulting fiber diameters from the various orifice orientations are shown in Table III. These results were obtained using an aqueous 6 wt. % PEO solution at 6000 rpm, with orifice diameters of 159 μm. The trend shows the fiber diameters decreasing as the angle of the orifice goes from facing opposite of rotation to facing the direction of rotation. However, an exception to this trend is seen with the straight needle, for which the smallest diameters were obtained. The attributing factors for the orifice analysis that affects the fiber diameters include the volumetric flow, the exiting velocity, and the shape of the exiting jet.

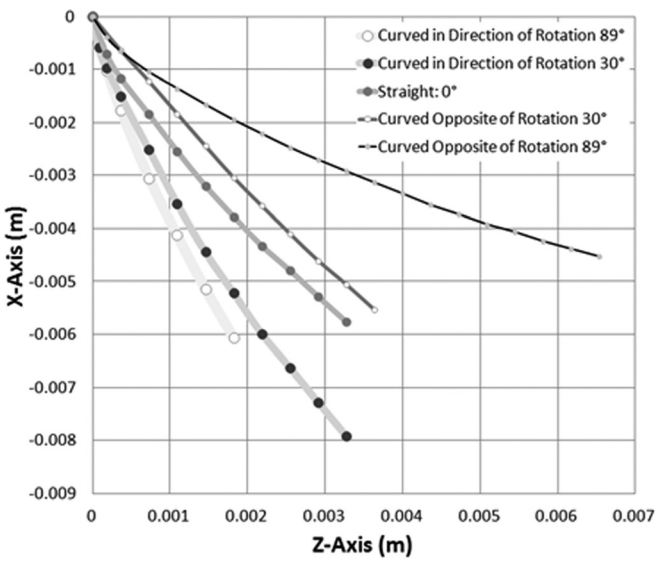

FIG. 12. Initial fiber trajectories with varying orifice exit angles.

TABLE III. Fiber diameters at varying orifice orientations using 6 wt. % PEO, forcespun at 6000 rpm.

Orifice orientation	Average fiber diameters (nm)	Sample standard deviation (nm)
Angled 89° opposite of rotation	**420**	**140**
Angled 30° opposite of rotation	**280**	**85**
Angled 30° in direction of rotation	**250**	**90**
Angled 89° in direction of rotation	**180**	**45**
Straight	**130**	**30**

Another parameter associated with the orifice that was studied was the aspect ratio, $L/2\,r$, where L is the distance within the spinneret that has the radius of the orifice, r. To vary the aspect ratio, needles with lengths of 0.635 cm, 1.27 cm, 1.905 cm, and 2.54 cm were used with an orifice diameter of 260 μm; this translates to aspect ratios of 24.4, 48.8, 73.2, and 97.6, respectively. Varying the aspect ratio did not affect the shape of the jet at exit, although the resulting trajectories were significantly affected, as shown in Figure 13. The shorter the needle, the more outward the fluid is expelled. This shows that increasing the aspect ratio reduces the exit velocity of the fluid, contracting the trajectory of the fiber. Using Eq. (5), to determine the change in exit velocity based on needle length, L, it is calculated that initially increasing the length of the needle reduces the exit velocity even as the overall radius of the spinneret is increased due to head losses experienced, and thus the fiber trajectory is contracted as seen in the experiments. The resulting fiber diameters, shown in Table IV, show that decreasing the aspect ratio, in this case through the reduction in needle length, reduces the final fiber diameters, but not significantly.

Forcespinning systems have been created with and without continuous feeding capabilities. For those without continuous feeding, a certain amount of fluid is inserted into the spinneret. As the material is forcespun, fluid depletion occurs that in turn has some effect on the fiber trajectory and final fiber diameters. To study these effects, the spinneret was filled with varying amounts of solution: 0.25 ml, 0.5 ml, 0.75 ml, and 1.0 ml. The variation of fluid fill level can also be seen as changing the flow rate of the solution since the flow rate is related to the pressure of the container caused by

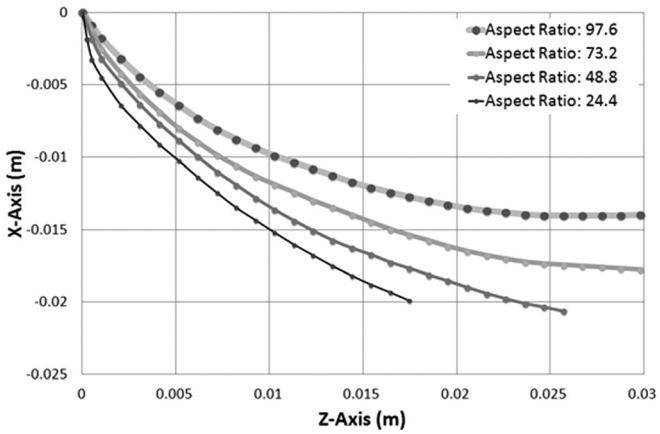

FIG. 13. Fiber trajectories with varying aspect ratios.

TABLE IV. Fiber diameters at varying aspect ratios using 6 wt. % PEO, forcespun at 6000 rpm.

Aspect ratio L/2 r	Average fiber diameters (nm)	Sample standard deviation (nm)
40	**140**	**45**
160	**190**	**60**

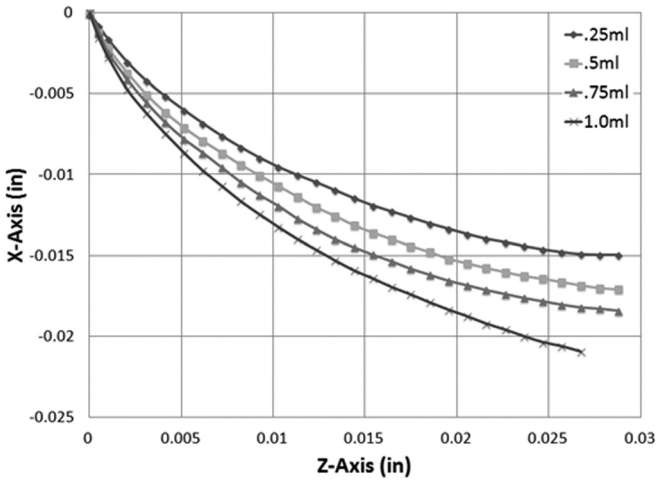

FIG. 14. Fiber trajectories with varying fluid fill.

the amount of fluid present. Increasing fluid fill level increases the flow rate. The resulting trajectories of each are shown in Figure 14. The trajectories show that as fluid fill level increases, the fiber is expelled further outward. The effects on fiber diameter, shown in Table V, show that as less fluid is available in the container the fibers grow in diameter, and the sample standard deviation is increased.

The effects of changing the orifice diameter on the final fiber diameter are shown by our research group.[10] They show that decreasing the orifice diameter decreases the final diameter of the collected fibers. Studying the effects of the various controllable parameters in FS, it was found that the two most influential parameters are the angular velocity of the spinneret and the viscosity of the material. This was followed by the orifice orientation and then by aspect ratio and fluid fill. It was also determined that expanding the fiber trajectory produces smaller fiber diameters in all cases with the exception of orifice orientation, where the straight needle was found to produce the smallest fiber diameters. The trends seen in this work are found to agree with modeling work reported on the determination of fiber diameter and trajectory for a simple inviscid case.[11]

TABLE V. Fiber diameters with varying fluid fill using 6 wt. % PEO, forcespun at 6000 rpm.

Fluid fill(ml)	Average fiber diameters (nm)	Sample standard deviation (nm)
0.25	**190**	**60**
1.0	**130**	**30**

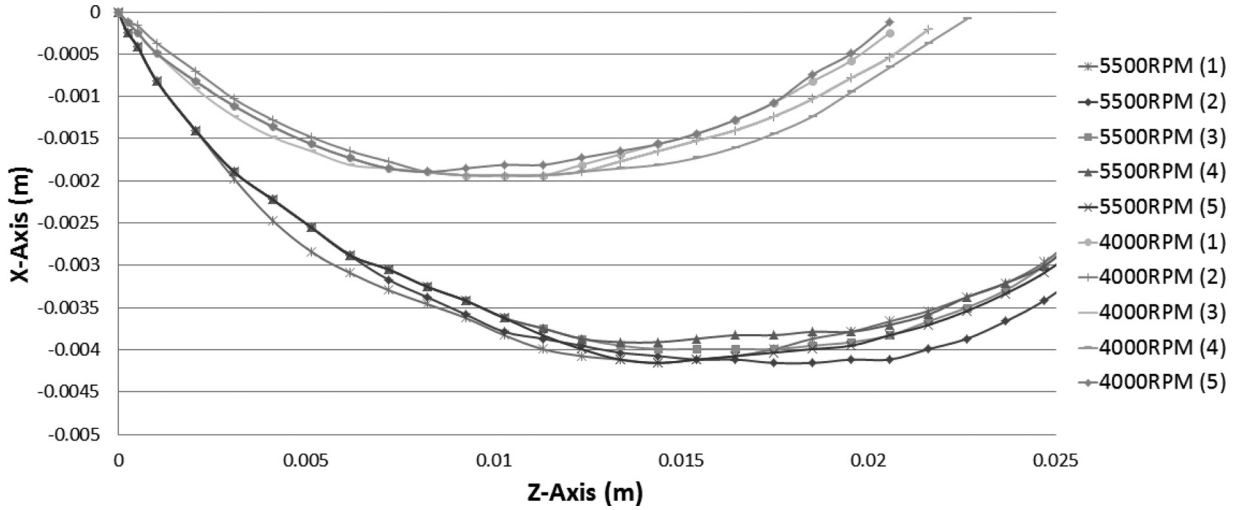

FIG. 15. Variance of fiber trajectories under the same conditions.

1. Trajectory variation

To determine the path variation of the trajectories plotted, multiple trajectories using the same parameters were obtained and compared. Figure 15 shows the path variation of the trajectories made by 6 wt. % PEO solution at 4000 rpm and 5500 rpm. Five different trajectories were obtained under the same conditions for each angular velocity. At large fiber lengths or far distance from the spinneret orifice the trajectories become chaotic and have large variations; however, at short lengths and close to the orifice the jet trajectories are found to be very stable with variations of ± 0.87 mm from the average trajectory. Due to the very small variations in trajectory at small fiber lengths, the trajectory results in part C can be seen as reproducible with negligible variations for the purpose of comparing the FS parameter effects.

IV. CONCLUSIONS

High speed photography was used to provide an insight into the mechanisms involved in the production of nanofibers through forcespinning. Magnified high speed captures were used to determine what occurs during the initial stages of fiber formation, and the jet shape required for nanofiber formation was established. Detailed information on the propagation of the produced fibers as they approach the collector was obtained and the mechanisms involved during FS were identified, providing the required information to develop a more thorough understanding of the FS fiber formation process. Controllable parameters were also studied to determine the effects that they have on the fiber formation. The results provided an insight into the nanofiber formation that will help in optimizing the nanofiber development. In all, the data gathered, regarding the mechanisms involved for forcespinning fiber formation and the effects of various controlled parameters provide a thorough understanding of this new nanofiber production method.

ACKNOWLEDGMENTS

This work was supported by National Science Foundation under DMR Grant Nos. 0934157 (PREM-The University of Texas Pan American (UTPA)/University of Minnesota - Science and Engineering of Polymeric and Nanoparticle-Based Materials for Electronic and Structural Applications) and 1040419 (MRI: Acquisition of an ESEM).

[1]T. Jarusuwannapoom, W. Hongrojjanawiwat, S. Jitjaicham, L. Wannatong, M. Nithitanakul, C. Pattamaprom, P. Koombhongse, R. Rangkupan, and P. Supaphol, Eur. Polym. J. **41**, 409 (2005).
[2]K. Sarkar, C. Gomez, S. Zambrano, M. Ramirez, E. de Hoyos, H. Vasquez, and K. Lozano, Mater. Today **13**(11), 12–14 (2010).
[3]S. Ramakrishna, K. Fujihara, W.-E. Teo, T. C. Lim, and Z. Ma, *An Introduction to Electrospinning and Nanofibers* (World Scientific, Singapore, 2005).
[4]X. M. Mo, C. Y. Xu, M. Kotaki, and S. Ramakrishna, Biomaterials **25**, 1883 (2004).
[5]T. Osswald and J. P. Hernández-Ortíz, *Polymer Processing-Modeling and Simulation* (Hanser, Germany, 2006).
[6]B. M. Boubnov and G. S. Golitsyn, *Convection in Rotating Fluids* (Springer, New York, 1995).
[7]C. W. Macosko, *Rheology: Principles, Measurements and Applications* (Wiley-VCH, 1994).
[8]S. Padron, R. Patlan, J. Gutierrez, N. Santos, T. Eubanks, and K. Lozano, J. Appl. Polym. Sci. **125**(5), 3610–3616 (2012).
[9]P. Mellado, H. A. McIlwee, M. R. Badrossamay, J. A. Goss, L. Mahadevan, and K. K. Parker, Appl. Phys. Lett. **99**, 203107 (2011).
[10]A. Altecor, Y. Rane, N. Bell, K. Lozano, "Preparation of superhydrophobic Teflon® AF 1600 sub-micron fibers and yarns using the Forcespinning™ Technique," J. Eng. Fibers Fabrics (submitted).
[11]D. I. Caruntu, S. Padron, K. Lozano, and A. A. Fuentes, "2-D modeling of Forcespinning™ fluid dynamics for fiber formation," Phys. Fluids (submitted).